J Solid State Electrochem (2011) 15:253–257
DOI 10.1007/s10008-010-1113-x

ORIGINAL PAPER

Reaction control and long-term stability of partial methane oxidation over an oxygen membrane

Alexey A. Markov · Mikhail V. Patrakeev · Ilia A. Leonidov · Victor L. Kozhevnikov

Received: 28 April 2010 / Revised: 24 May 2010 / Accepted: 26 May 2010 / Published online: 6 June 2010

Abstract In this paper, peculiarities are discussed of the temperature control of the methane partial oxidation (POM) in the laboratory reactor with oxygen separating the tubular membrane of lanthanum–strontium ferrite. It is shown that reactions at the catalyst may result in the local decrease of the temperature. Therefore, correct monitoring of the heat regime of the process is possible only when direct contact is avoided of the catalyst with controlling thermocouple. The long-term testing showed stable performance characteristics of the entire POM system during more than 7000 h with the methane conversion level and selectivity of no less than 98.8% and 90%, respectively.

Keywords Oxygen separating membranes · Mixed conducting oxides · Partial oxidation · Catalytic reactor · Synthesis gas · Methane · Hydrogen · Selectivity · Conversion

Introduction

The using of mixed, oxygen ion and electron, conductivity oxides (MIECs) as ceramic membranes for the integrated process of oxygen separation and partial oxidation of methane to syngas is currently considered as one of the most advantageous and cost-efficient MIEC applications. The driving force for the transport of oxygen is a difference in oxygen activity between the feed and permeate sides of the membrane. As a result, oxygen permeates from the side with high oxygen activity to the side with low activity. On the feed side surface of the membrane, the adsorbed oxygen molecules reduce to two oxide ions $O_2 \rightleftarrows 2O^{2-} + 4e^-$. This oxide ions migrate through a thermally activated hopping mechanism to the permeate side surface of the membrane where they can either directly interact with adsorbed methane molecules or recombine and desorb, thus supporting reactions with methane in the gas phase. Simultaneously, electrons drift from the permeate side to the feed side, thus serving to short circuit the membrane and ensure its electrical neutrality. Depending on the prevailing reaction mechanism (surface or gas phase), different arrangements of the catalyst can be used at the membrane permeate side. Therefore, the respective device can be characterized as a combined electrochemical–catalytic membrane reactor. More details concerning scientific foundations of the relevant transport phenomena are considered in work [1]. Authors [2] report on economic aspects of the emerging technology. However, particular emphasis in recent years has been given to development [3–10] and testing of membrane materials [10–18]. Still, the achieved lifetime of MIEC membranes is not sufficient for their wide introduction in practice. It is worth noticing that, though the durability of membranes is influenced to a degree by structural features and defect architecture, it seems to depend most considerably on their chemical composition that often includes large amounts of easily reducible oxides of 3d row end metals such as Co or Cu [19–21]. On the other hand, ferrous materials, i.e., based on more stable iron oxide, have not only appreciable mixed conductivity but also exhibit a rather more suitable combination of service properties (thermodynamic stability, moderate thermal and chemical expansion, etc.). We have shown earlier that

Dedicated to Prof. R. Schöllhorn on his 75th birthday

A. A. Markov · M. V. Patrakeev (✉) · I. A. Leonidov · V. L. Kozhevnikov
Institute of Solid State Chemistry,
Ural Branch of Russian Academy of Sciences,
91 Pervomaiskaya Str.,
Yekaterinburg, Russia
e-mail: patrakeev@ihim.uran.ru

lanthanum–strontium ferrite $La_{0.5}Sr_{0.5}FeO_{3-\delta}$ (LSF) can be successfully utilized as a membrane material for oxygen separation in the POM process [22]. In continuation of these studies, the focus in the present work is on the thermal regime and long-term stability of the POM reactor.

Experimental

The powder of LSF was prepared by glycine nitrate synthesis [23]. The typical procedure was as follows: The high-purity nitrates taken in desirable proportions were dissolved in distilled water at moderate heating. Then, amino acetic acid was added to the nitrates in double excess. The gradual heating resulted in thickening and ignition of the desiccated material. The combustion product was ground and subjected to calcination at 1000–1200°C for 10 h. X-ray powder diffraction was used to confirm single-phase final products. The synthesized powders with the average grain size of about 1 μm were mixed with commercial paraffin at 70–80°C and cooled down to room temperature. The batch was separated in small pieces to be fed in a Haake Polidrive extruder with tubing die. The extruded green body was dried at 200°C in order to remove the paraffin, and then temperature was slowly increased to 1250–1300°C. The firing time was 5 h. The wall thickness and external diameter of the obtained tubular ceramic membranes were about 1 and 10 mm, respectively. The density was 95–97% of the theoretical value. In order to verify the absence of microcracks, the obtained ceramic tube was attached to the pressurized air line and checked on air leaks by submerging in ethanol.

Alumina ceramic cylinders with a diameter and length of 2 and 6–10 mm, respectively, were used as catalytic support. The support was soaked in a water solution of nickel nitrate, dried, and fired at 1000°C to form the catalysts with the nickel metal load of about 10% wt.

The experimental setup for POM tests is shown in Fig. 1. The reactor encasement was made of quartz tube with the diameter and length of 40 and 700 mm, respectively. The butt ends of the encasement were covered with flanges and equipped with alumina tubes for air passage. The oxygen membrane under test was sealed in between upper and lower supporting auxiliary alumina tubes. The typical length of the membrane for regular tests was 50 mm. In order to reduce feed gas consumption, 20-mm membranes were used in long-term stability tests. The spacing between encasement and membrane was filled with the catalyst. The Bronkhorst mass flow controllers were used for the preparation and measurement of the inlet feed gas. The outlet stream was passed through the condenser in order to remove water vapors, and then a gas chromatograph was used for the analysis of volume concentrations (x_i) of different gases in the outlet stream. In the preliminary work [22], the furnace temperature was controlled only. In order to gain a deeper understanding of temperature variations across the reactor in this study, we used S-type thermocouples Tc1, Tc2, and Tc3 set at different check points where the respective temperature values, T_1, T_2, and T_3, were read with the help of a Keithley 2000 digital multimeter. Yokogawa UT-155 controller was used for temperature maintenance of the furnace. A personal computer with specially developed software was used for running the experiments and data processing. The catalyst at the membrane outside was flashed with argon (purge gas) during 5 h upon achieving experimental temperature, and then methane was gradually added in the stream so that in 20 h the argon feed was completely replaced with methane. Based on the data of the outlet gas analysis, the POM process was characterized with conversion (X_{CH_4}), selectivity (S_{CO}), hydrogen-to-carbon monoxide ratio (H_2/CO), and oxygen separation flux density (J_{O_2})

$$X_{CH_4} = \left(1 - \frac{x_{CH_4}}{x_{CO} + x_{CO_2} + x_{CH_4}}\right) \times 100\% \quad (1)$$

$$S_{CO} = \left(\frac{x_{CO}}{x_{CO} + x_{CO_2}}\right) \times 100\% \quad (2)$$

$$J_{O_2} = F_d^{out} \times \left(1.5x_{CO} + 2x_{CO_2} + x_{O_2} - 0.5x_{H_2} - \frac{0.21}{0.78}x_{N_2}\right)/s \quad (3)$$

Here, F_d^{out} is the flow of the dry outlet gas, 0.21 and 0.78 are volume fractions of oxygen and nitrogen in air, respectively, s is membrane surface, and the last term accounts for nitrogen leaks through microcracks and imperfections in seals. Since conversion exceeded 98% in all experiments, this parameter is not shown in the plots below.

Results and discussion

Ferrite $La_{0.5}Sr_{0.5}FeO_{3-\delta}$ is characterized by highest ambipolar conductivity in the series of solid solutions $La_{1-x}Sr_xFeO_{3-\delta}$ [24, 25], and the calculated oxygen permeation flux density through 1-mm-thick membrane of this oxide can achieve 8 $ml \times min^{-1} \times cm^{-2}$ at 900°C when the permeate side oxygen partial pressure is 10^{-16}atm while the other side is flushed with air. On the other hand, some limitations on the flux can be imposed by surface reactions [26]. It is interesting, therefore, to observe the oxygen separation efficiency of this material in conditions of a real

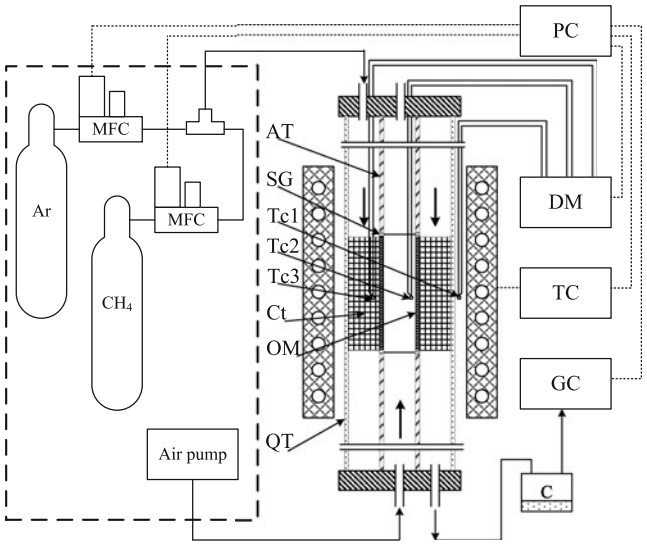

Fig. 1 The sketch of the experimental setup. *MFC*, mass flow controller; *PC*, personal computer; *DM*, digital multimeter; *TC*, temperature controller; *GC*, gas chromatograph; *C*, condenser; *AT*, alumina tube; *SG*, sealant glass; *Tc1, Tc2, and Tc3*, thermocouples; *Ct*, catalyst; *OM*, oxygen membrane; *QT*, quartz tube

POM process. The conversion parameters at 900°C versus methane flow are shown in Fig. 2. Notice that temperature was set with the help of thermocouple Tc1 in the spacing between reactor encasement and external heaters. Surprisingly, experimentally achieved flux density of about 10 ml×min^{-1}×cm^{-2} exceeded the calculated value. Hence, the temperature of the membrane was probably higher than 900°C.

In order to better understand temperature regimes in different areas, thermocouples Tc2 and Tc3 were located near membrane inside and outside surfaces, i.e., in air and methane streams, respectively (Fig. 1). The heating power was supplied so that temperature would not exceed 950°C, and when this upper limit was achieved either at Tc2 or at Tc3 respective thermocouple was used for temperature maintenance. The temperature changes at check points and conversion parameters versus methane flow are shown in Fig. 3. It is seen that T_2 is lower than T_3 at F_{CH_4}< 20 ml×min^{-1}, which is due to colder inlet air and insufficiently intensive heat transfer through the catalytic bed. However, a further increase of methane flow results in faster temperature increase at Tc2, and the air stream temperature approaches 950°C near F_{CH_4}= 40 ml×min^{-1} while the temperature in the catalytic bed progressively decreases. These results suggest that the low selectivity at moderate values of the methane flow reflects a considerable development of the total oxidation reaction

$$CH_4 + 2O_2 \rightleftarrows CO_2 + 2H_2O + 802\ kJ \tag{4}$$

which is characterized with a very large heat effect. On the other hand, the selectivity increase with methane flow (Fig. 3) gives evidence to the increasing impact of the partial oxidation reaction

$$CH_4 + \frac{1}{2}O_2 \rightleftarrows CO + 2H_2 + 44\ kJ \tag{5}$$

Hence, the enthalpy for the combination of reactions (4) and (5) is

$$\Delta H_\Sigma = S_{CO} \times 44\ \text{kJ} + (1 - S_{CO}) \times 802\ \text{kJ} \tag{6}$$

Then, the dependence of specific heat power on methane flow in the reactor can be found as

$$P = \Delta H_\Sigma \frac{F_{CH_4}}{22.4\text{l} \times \text{mol}^{-1} 60} X_{CH_4} \tag{7}$$

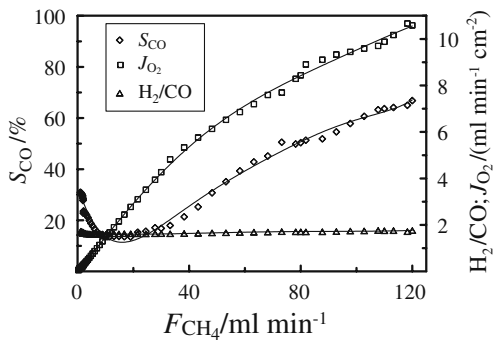

Fig. 2 Performance characteristics of the tubular LSF membrane versus feed flux at T_1=900°C. The surface of membrane is 12.5 cm^2; the flow rate of air is 1000 ml×min^{-1}

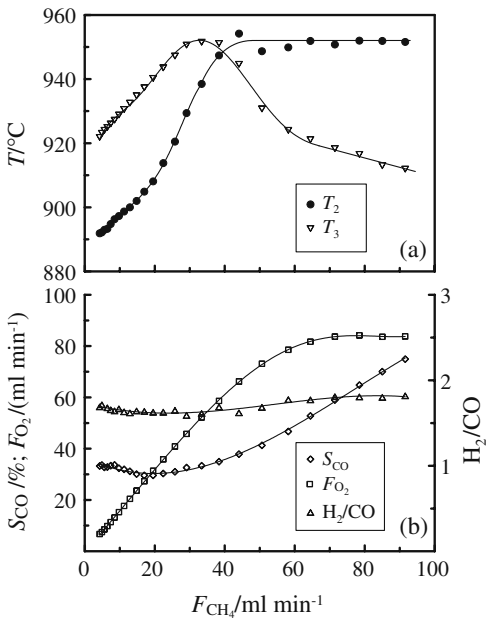

Fig. 3 Temperature readings of thermocouples Tc2 and Tc3 (see text) and performance characteristics of the tubular LSF membrane versus feed flux

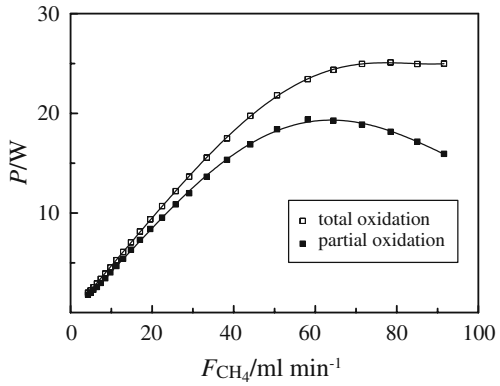

Fig. 4 The heat power released at the membrane surface and overall heat power

Here, 22.4 mol^{-1} is molar volume, and 60 is a factor for conversion of minutes to seconds. The results are shown in Fig. 4 as calculated from experimental values of selectivity in Fig. 3. As expected, the heat output increases with methane flow up to 15–18 kJ at 40–60 ml×min^{-1} and then begins to decline. At the same time, specific heat power calculated at zero selectivity, i.e., when all permeate oxygen is exhausted in the reaction of total oxidation, achieves saturation. The heat power difference clearly demonstrates that the summary reaction in the tubular reactor (Fig. 1) evolves mainly as total methane oxidation, most probably in a thin gas layer near the membrane surface, followed by reactions of combustion products with methane over a catalytic bed where a large amount of heat is consumed. This picture gives a simple explanation to the observed high efficiency of ordinary nickel catalysts that are widely used for steam/carbon dioxide reforming. It follows also from the obtained results that a more precise control of membrane working conditions can be carried out with the help of thermocouple Tc2 located directly at the membrane feed side.

From a practical standpoint, the longevity of the separating membrane in the reforming process is probably the most important issue. The variations of the POM parameters versus time at 950°C are shown in Fig. 5. The selectivity of about 80% was attained at the end of the transitory period of replacement of the purge gas for pure methane while oxygen permeation flux density achieved nearly 6.8 ml×min^{-1}×cm^{-2}. This value is in agreement with the flux calculated from conductivity [22] when the permeate side oxygen partial pressure equals $10^{-8.5}$atm. A fast increase of nitrogen concentration in the outlet gas after 220 h signals the development of cracks either in seals or in the membrane. The subsequent inspection of the disassembled reactor confirmed membrane degradation. The temperature decrease to 850°C resulted in a respective decrease of the oxygen permeate flux density to 3 ml×min^{-1}×cm^{-2}. On the other hand, the calculated flux should be near 4 ml×min^{-1}×cm^{-2}. This difference suggests that temperature decrease from 950 to 850°C results in the development of surface exchange limitations. This conclusion is corroborated with the results of [27] where it was observed that oxygen fluxes through 1- and 1.6-mm membranes of $La_{0.5}Sr_{0.5}FeO_{3-\delta}$ did not differ at 800°C and thus evidenced surface exchange control over oxygen transport. However, much better membrane performance was achieved. It is seen from Fig. 6 that conversion parameters remained fairly stable for about 7500 h at selectivity near 92%. The after-test EDX analysis did not reveal any chemical changes across the membrane, and X-ray analysis confirmed the phase integrity of the material.

The obtained results demonstrate that the optimal working temperature for the ferrite membranes is between 850 and 900°C. The oxygen permeation within these limits depends on the interplay of bulk oxygen chemical diffusion and surface oxygen exchange kinetics. At the same time, kinetic demixing and related phase instabilities [28] do not seem to play any role in the lifetime of the membrane.

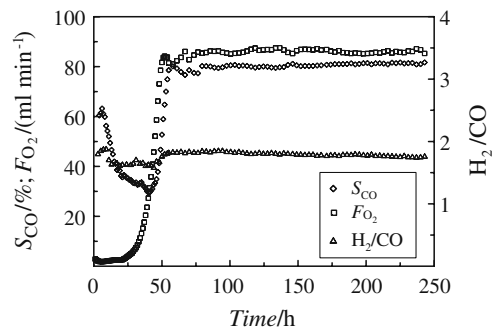

Fig. 5 Performance characteristics of the tubular LSF membrane at 950°C. The surface of membrane is 12.5 cm^2; the flow rate of air is 1000 ml×min^{-1}

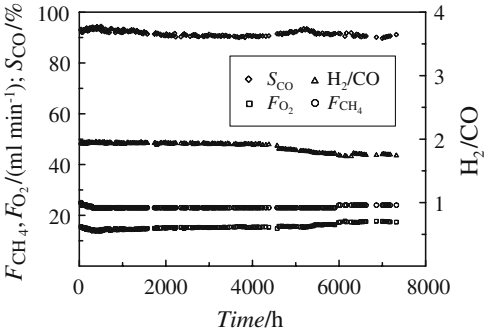

Fig. 6 Performance characteristics of the tubular LSF membrane at 850°C. The surface of membrane is 5 cm^2; the flow rate of air is 300 ml×min^{-1}

Conclusion

In general, we have shown that perovskite-like ferrites are promising materials for oxygen separating membranes to be used in an electrochemical POM reactor. A reasonable compromise of permeability and stability can be achieved by fine-tuning of the chemical composition of the material and precise control of the membrane temperature. Surface-controlled kinetics affects noticeably upon oxygen permeation of the membranes at temperatures below 850°C. Structural instabilities related to kinetic demixing or chemical reactions of the membrane with gaseous components do not develop considerably at this temperature, thus providing longevity of the membrane. The arguments are given in proof of the reforming mechanism that involves total oxidation of the sweep methane with oxygen permeate followed by the interaction of the oxidation products, i.e., water vapor and carbon dioxide, with methane. Therefore, well-developed nickel–alumina catalysts for steam reforming can be used efficiently in a POM reactor.

Acknowledgments Authors are grateful to the Presidium of the Ural Branch of RAS for the partial support of this research.

References

1. Bouwmeester HJM, Burgraaf AJ (1996) Fundamentals of inorganic membrane science and technology. In: Burgraaf AJ, Cot L (eds). Elsevier, Amsterdam
2. Bredesen R, Sogge J (1996) A technical and economic assessment of membrane reactors for hydrogen and syngas production. In: Seminar on the ecological applications of innovative membrane technology in the chemical industry. Economic Commission for Europe, United Nations, Chetraro, Calabria, Italy
3. Mazanec TJ (1997) Electropox gas reforming. In: Anderson HU, Khandar AC, Liu M (eds) Ceramic membranes I. The Electrochemical Society, Penington, NJ, PV95-24, pp 16–28
4. Hendriksen PV, Larsen PH, Mogensen M, Poulsen FW, Wilk K (2000) Catalisis Today 56:283–295
5. Sammells AF, Schwarz M, Mackay RA, Barton NF, Peterson DR (2000) Catal Today 56:325
6. Dong H, Shao ZP, Xiong GX, Tong JH, Sheng SS, Yang WS (2001) Catal Today 67:3
7. Bouwmeester HJM (2003) Catal Today 82:141–150
8. Diethelm S, Sfeir J, Clemens F, van Herle J, Favrat D (2004) J Solid State Electrochem 8:611–617
9. Thursfield A, Metcalfe IS (2006) J Solid State Electrochem 10:604–616
10. Caro J, Wang HH, Tablet C, Kleinert A, Feldhoff A, Schiestel T, Kilgus M, Kölsch P, Werth A (2006) Catal Today 118:128–135
11. Tong J, Yang W, Suda H, Haraya K (2006) Catal Today 118:144–150
12. Leonidov IA, Kozhevnikov VL, Mitberg EB, Patrakeev MV, Kharton VV, Marques FMB (2001) J Mater Chem 11:1201–1208
13. Park CY, Jacobson AJ (2005) J Electrochem Soc 152:J65–J73
14. Kharton VV, Shaula AL, Snijkers FMM, Cooymans JFC, Luyten JJ, Marozau IP, Marques FMB, Frade JR (2006) J Eur Ceram Soc 26:3695–3707
15. Balachandran U, Ma BH (2006) J Solid State Electrochem 10:617–624
16. Zhu X, Wang HH, Cong Y, Yang W (2006) Catal Lett 111:179–185
17. Søgaard M, Hendriksen PV, Mogensen M (2007) 1489–1503
18. Markov AA, Savinskaya OA, Patrakeev MV, Nemudry AP, Leonidov IA, Pavlyukhin YT, Ishchenko AV, Kozhevnikov VL (2009) J Solid State Chemistry 182:799–806
19. Ito W, Nagai T, Sakon T (2007) Solid State Ionics 178:809–816
20. Zhang H, Dong X, Lin W (2006) Nat Gas Ind 26:155–157
21. Hu J, Xing T, Jia Q, Hao H, Yang D, Guo Y, Hu X (2006) Appl Catal A: Gen 306:29–33
22. Kozhevnikov VL, Leonidov IA, Patrakeev MV, Markov AA, Blinovskov YN (2009) J Solid State Electrochem 13:391–395
23. Chick LA, Pederson LR, Maupin GD, Bates JL, Thomas LE, Exarhos GL (1990) Mater Lett 10:6–12
24. Patrakeev MV, Bahteeva JA, Mitberg EB, Leonidov IA, Kozhevnikov VL, Poeppelmeier KR (2003) J Solid State Chem 172:219–231
25. Diethelm S, van Herle J, Sfeir J, Buffat P (2005) J Eur Ceram Soc 25:2191–2196
26. Ramos T, Atkinson A (2004) Solid State Ionics 170:275–286
27. Tsipis EV, Patrakeev MV, Kharton VV, Yaremchenko AA, Mather GC, Shaula AL, Leonidov IA, Kozhevnikov VL, Frade JR (2005) Solid State Sci 7:355–365
28. Atkinson A, Ramos TMGM (2000) Solid State Ionics 129:259–269